DUST AND THE FAR-UV SPECTRAL ENERGY DISTRIBUTION OF QUASARS

Luc Binette,[1] Yair Krongold,[1] Gladis Magris Crestini[2] and Jose Antonio de Diego[1]

RESUMEN

La distribución de energía espectral de los cuasáres presenta un empinamiento abrupto del continuo a longitudes más cortas que $\simeq$ 1100 Å. Presentamos un nuevo modelo de extinción por polvo constituido de granos de carbono cristalino. Analizamos las propiedades en extinción poco usuales de este polvo y demostramos como el empinamiento abrupto observado en cuásares puede ser modelizado exitosamente por polvo hecho de carbono cristalino.

ABSTRACT

The spectral energy distribution of quasars shows a sharp steepening of the continuum shortward of $\simeq$ 1100 Å. We present a new dust extinction model consisting of crystalline carbon grains. We analyze the unusual extinction properties of this dust and proceed to show how the observed UV spectral break can be successfully modelled by crystalline carbon dust.

Key Words: **ISM: DUST — GALAXIES: ACTIVE — RADIATIVE TRANSFER — ULTRAVIOLET: GENERAL**

1. INTRODUCTION

The ultraviolet energy distribution of quasars is characterized by the so-called "big blue bump", which peaks in νF_ν at approximately 1000 Å. The quasar 'composite' spectral energy distribution (SED) of Telfer et al. (2002, hereafter TZ02) obtained by co-adding 332 HST-FOS archived spectra of 184 quasars between redshifts 0.33 and 3.6, exhibits a steepening of the continuum at $\sim$ 1100 Å. A fit of this composite SED using a broken powerlaw reveals that the powerlaw index changes from -0.69 in the near-UV to -1.76 in the far-UV (see TZ02). We label this observed sharp steepening the 'far-UV break'. In these proceedings, we first give a short overview of our classification of the HST-FOS quasar spectra based on the appearance of the far-UV break. We then describe our dust absorption model based on crystalline carbon grains. We illustrate the extinction properties of this dust and proceed to compare with two quasar spectra. In a previous proceeding (Binette et al. 2005b), we described how we came to consider the possibility of carbon crystallite dust. The argumentation in support of the dust absorption interpretation of the UV break has been fully described in Binette et al. (2005a, hereafter BM05). Complementary information about crystalline dust can be found in this and other proceedings (Binette et al. 2005b, 2006).

2. CLASSIFICATION OF THE FAR-UV BREAK APPEARANCE

The concept of a 'composite' Spectral Energy Distribution (SED) that extends into the far-UV rests on the redshift effect, which allows us to observe the far-UV region of high-$z$quasars, beyond the Lyman limit, even though our Galaxy is highly opaque in this wavelength region (observer-frame). For the concept of a 'composite' SED obtained by averaging to work, the environment of quasars must be highly transparent beyond the Lyman limit, a condition which is generally satisfied for quasars at $z_q \lesssim 3.6$. In what follows, we will consider the sample of HST-FOS spectra that H. Telfer kindly lent to us. These have already been corrected for Galactic dust extinction, for the presence of the Lyman valley due to unresolved Lyα forest lines and for the presence of Lyman limit systems. Of all the spectra available, we consider only those 106 quasars for which more than one grating was used since otherwise the λ_{rest} coverage turned out to be too narrow to provide meaningful constraints to the models. Furthermore, only 61 of these spectra extend sufficiently in the far-UV (900 Å) to reveal enough of the far-UV break to be of use to us.

After reviewing the HST-FOS sample, some patterns emerge among the selected 61 multigrating spectra. The majority of them (44 quasars) resemble the composite SED of TZ02. We classify those

[1]Instituto de Astronomía, UNAM, México D.F., México.
[2]Centro de Investigaciones de Astronomía, Mérida, Venezuela.

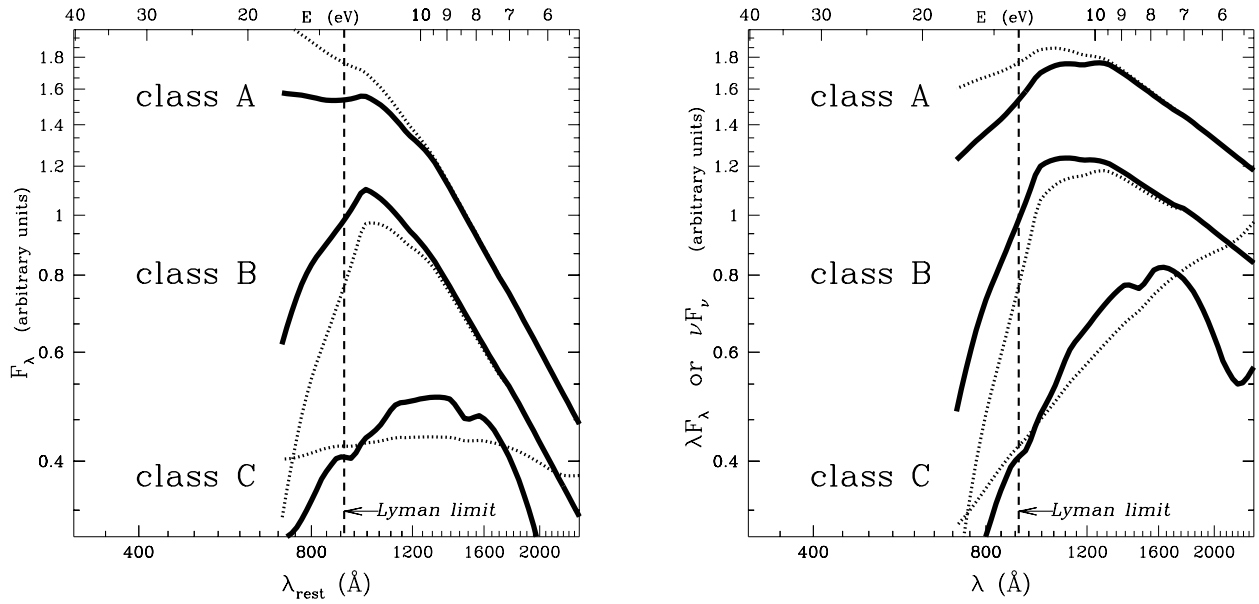

Fig. 1. Panel a (left): cartoon that illustrates in F_λ the three main classes of far-UV break (continuous lines) observed among the 61 multigrating HST-FOS spectra that extend down to at least 900 Å. The dotted line shows typical variations within a given class. Panel b (right): same descriptive cartoon using instead the νF_ν representation.

as class (A). Others (6 quasars) show a sharper and much more pronounced break. We label these class (B). Eight other quasars present a somewhat shallower break, which appears to start further in the near-UV or to present a SED which is flat throughout the F_λ region covered. A cartoon of theses three classes is presented in Fig. 1a. The dotted lines show typical variations within each class. Finally, only 3 quasars did not fit any meaningful pattern (class D). In Fig. 1b, we show the same cartoon, but in νF_ν ($= \lambda F_\lambda$). We found the traditional F_λ representation of Fib. 1a. to be more appropriate and useful when fitting the UV break region.

3. THE EXTINCTION CURVE PRODUCED BY CRYSTALLINE CARBON

At the onset of our project, it became clear that ISM or even SMC-like dust could not reproduce a break as sharp as the one observed in the far-UV of quasars. Such a conclusion had been reached by Shang et al. (2005). A bibliographical research indicated that crystalline carbon might possess the required optical properties (Mutschke et al. 2004). Assuming spherical grains and the Mie theory, we used the subroutine BHMIE (Bohren and Huffman 1983) to compute the extinction curves, adopting the complex refraction indices $n + ik$ as tabulated in Mutschke et al. (2004) and in Edwards & Philipp (1985) . Crystalline carbon can appear either in a pure form or with surface impurities. In the former case, they are referred to as terrestrial cubic diamonds. In the latter case, nanodiamonds of the type

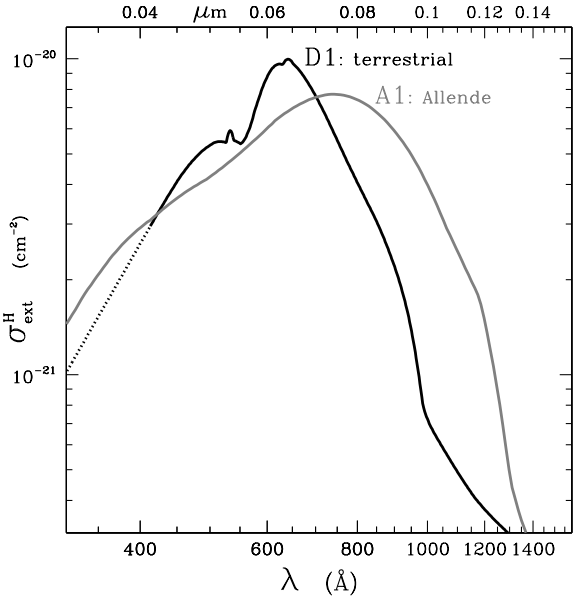

Fig. 2. Extinction cross section for nanodiamonds with and without surface impurities (A1 and D1, respectively). The small grain size regime was assumed. The complex refraction indices $n + ik$ used in the derivation of the extinction curves are from Mutschke et al. (2004) for the Allende meteorite nanodiamonds and from Edwards & Philipp (1985) for the cubic (terrestrial) nanodiamonds.

that are found in abundance in primitive meteorites will represent the case of crystalline C with impurities. Convincing evidence of nanodiamonds being detected in emission is provided by the 3.43 and 3.53 μm emission bands observed in two Ae/Be stars and one post-AGB star (see Van Kerckhoven, Tielens & Waelkens 2002). These bands result from the excitation of surface CH stretching modes (implying the existence of nanodiamonds with H surface impurities). We present in Fig. 2 the extinction curves A1 and D1 resulting from nanodiamonds with and without surface impurities. We assumed a powerlaw grain size distribution within the range 2 to 25 Å. It turns out that within this small grain size regime, using a log-normal distribution or altering slightly the above size limits do not produce any differences in the derived extinction curves, as explained in BM05.

It is apparent from Fig. 2 that the steepness of the *near-UV* extinction rise ought to produce a sharp absorption break, a desired feature for the any dust grain model that aims at fitting the UV quasar break. The extinction curves in Fig. 2 were normalized in such a way that they represent the case of having all the carbon in the dust (assuming a solar C/H abundance ratio). This normalization would need to be scaled according to the actual but unknown dust-to-gas ratio appropriate to the quasar environment.

4. POWERLAWS ABSORBED BY NANODIAMOND DUST

Where might the putative crystalline dust be located? In BM05, we present calculations in which the dust is either intrinsic to the quasars or intergalactic. In the end, we concluded that only the *intrinsic dust* hypothesis was satisfactory. The calculations presented here will assume the intrinsic dust case.

If one fits with a powerlaw the near-UV spectra of class (A) spectra, one finds that the average spectral index is $\bar{\alpha}_{NUV} = -0.44$ with a dispersion of 0.21. The corresponding histogram is shown in Fig. 4. This average considers only the 21 objects, for which a reliable estimate of α_{NUV} could be determined directly from the HST spectra. It is significantly harder than the mean value of -0.69 reported by TZ02 and the median value of -0.83 ± 0.04 for local AGN reported by Scott et al. (2004), presumably, because the softer class (C) spectra are not included in our average. In Fig. 5a and 5b, we present a powerlaw of index $\alpha_\nu = -0.4$ absorbed by nanodiamond dust of A1 and D1 types, respectively. The dust screen takes on four different thicknesses corresponding to H columns (in units of $10^{20}\,\mathrm{cm}^{-2}$) of

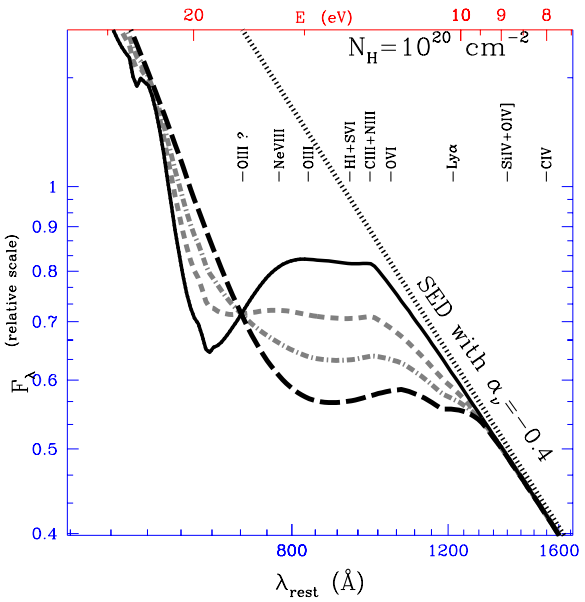

Fig. 3. Absorption models assuming a powerlaw SED of index $\alpha_\nu = -0.4$ (dotted line). The nanodiamond dust screen corresponds to an hydrogen column of $10^{20}\,\mathrm{cm}^{-2}$. The absorbed SED represented by the continuous line corresponds to pure cubic diamonds (D1) while the long dashed line corresponds to nanodiamonds from the Allende meteorite (A1). The grey lines correspond to a mixture of the two flavors: dashed line: 60% D1 + 40% A1, dot-dashed line: 30% D1 + 70% A1. Labelled pointers indicate where emission lines are expected in the rest-frame quasar spectra.

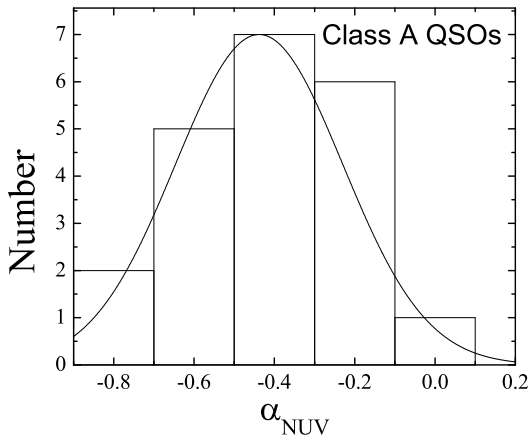

Fig. 4. Distribution of the near-UV powerlaw indices found among the 21 class (A) quasars for which a reliable estimate of α_{NUV} could be determined directly from the HST spectra.

$N_{20} = 0.5$, 1.0, 2.0 and 4.0. When $N_{20} \approx 1.0$, the

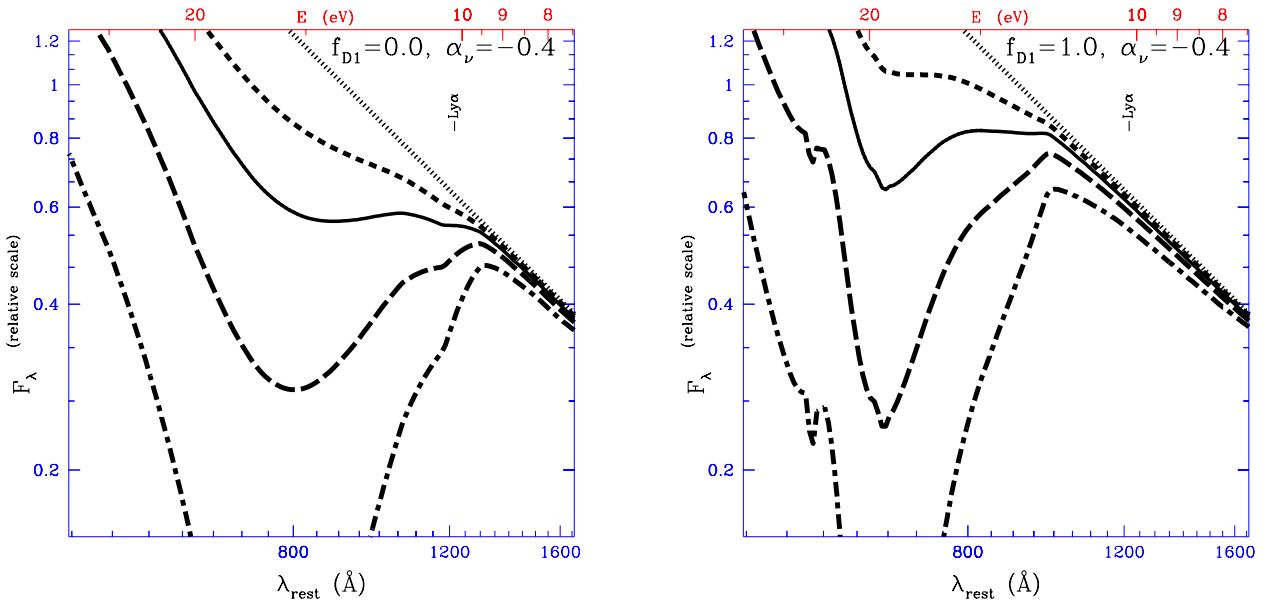

Fig. 5. Absorbed powerlaw SED assuming a constant index $\alpha_\nu = -0.4$ (dotted line) and the following H columns in units of 10^{20} cm^{-2}: N_{20} = 0.5, 1.0, 2.0 and 4.0. Panel a (left): terrestrial nanodiamond dust (D1). Panel b (right): meteoritic nanodiamonds (A1). (f_{D1} is the fraction of D1 dust).

absorption results in a near horizontal F_λ spectral segment shortward of the break. The position of the break occurs at different wavelengths, depending on the dust composition (compare Fig. 5a and 5b). It occurs longward and shortward of Lyα in the case of the A1 and D1 dust, respectively. Furthermore, terrestrial diamond dust can result in a conspicuous absorption dip near 650 Å (continuous line in Fig. 5b and 3), which may have some relevance to the narrow absorption dip reported by Scott et al. in their composite SED, which was interpreted as blueshifted Ne VIII absorption.

5. COMPARISON OF OUR MODELS WITH TWO QUASAR SPECTRA

In Fig. 6a and 6b, we present our absorbed powerlaw fit to the class (A) quasar PG 1008+1319 and to the class (B) quasar Pks 1229−02, respectively. In the case of PG 1008+1319, it is interesting to notice that the UV break is followed by a far-UV rise, which is well modeled by our nanodiamond dust model, using N_{20}=1.2 and a dust composition consisting of 70% of Allende nanodiamonds and 30% of cubic nanodiamonds (f_{D1}=0.30). The assumed spectral index is $\alpha_{NUV} = +0.13$, a value determined by Neugebauer et al. (1987). In the case of the class (B) quasar Pks 1229−02, the model shown in Fig. 6b assumes $\alpha_{NUV} = -0.4$ and is characterized by a column N_{20}=3.6 and dust composed mostly of cubic diamonds (D1) with f_{D1}=0.90.

It appears that the six class (B) quasars in our sample are not only more absorbed than class (A) but are extincted by dust dominated by cubic diamond grains (D1). On the other hand, the UV break in class (A) spectra generally requires a mixture of the two dust flavors. The absorption column is lesser in class (A) spectra. The break in 39 class (A) quasars is well reproduced using a column in the range $0.6 \leq N_{20} \leq 1.4$.

The authors acknowledge support from CONACyT grant 40096-F. We thank Randal Telfer for sharing the reduced HST FOS spectra. Diethild Starkmeth helped us with proofreading.

REFERENCES

Binette, L., Magris C., G., Krongold, Y., Morisset, C., Haro-Corzo, S., de Diego, J. A., Mutschke, H. & Andersen, A., 2005a, ApJ, 631, 661 (BM05)

Binette, L., Morisset, C., & Haro-Corzo, S., 2005b, in proc. of *The ninth Texas-Mexico Conference on Astrophysics*, April 13–16, 2005, in San Antonio, Texas, eds. S. Torres & G. MacAlpine, RevMexAA(SC), 23, 77

Binette, L., Mutschke, H., Andersen, A., Haro-Corzo, S., 2006, in Proc. of "Granada Workshop on High Redshift Radio Galaxies", Granada, 18–20 April 2005, Ed. M. Villar-Martín, E. Pérez, R. González-Delgado and J.L. Gómez, Astronomische Nachrichten, 327, 151

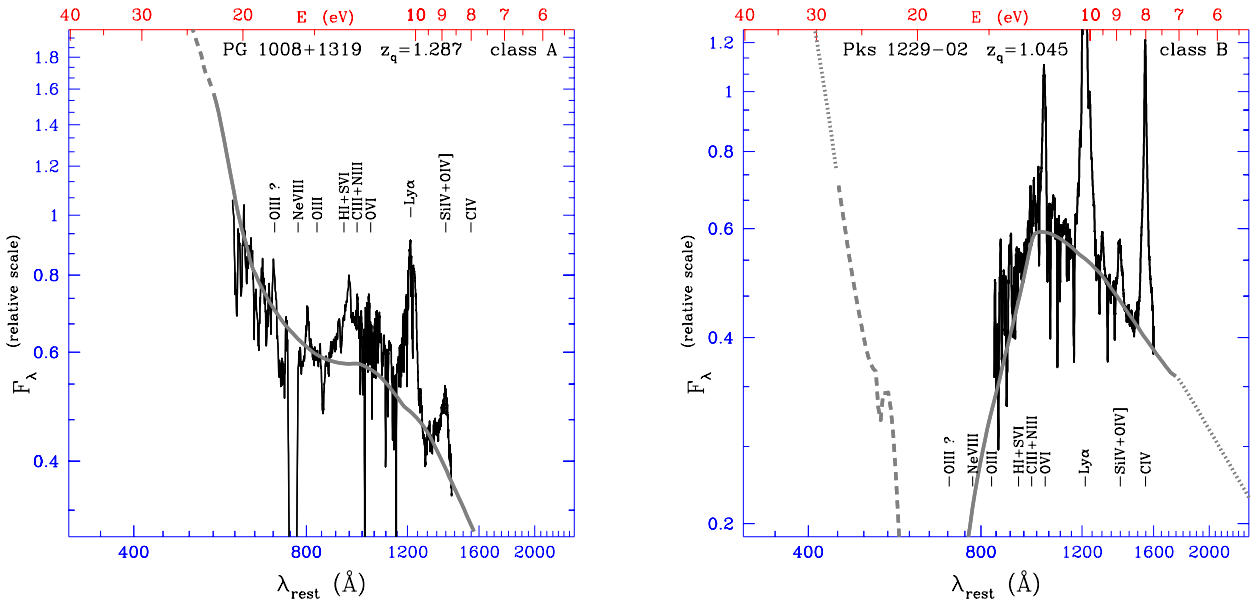

Fig. 6. Left panel a: rest-frame spectrum of class (A) quasar PG 1008+1319. Notice the far-UV rise shortward of the UV break. The model (grey line) assumes $\alpha_\nu = +0.13$, N_{20}=1.2 and f_{D1}=0.3. Right panel b: rest-frame spectrum of class (B) quasar Pks 1229−02. The model (grey line) assumes $\alpha_\nu = -0.4$, N_{20}=3.6 and f_{D1}=0.90. This is the largest column encountered among classes (A+B).

Bohren, C. F. & Huffman, D.R. 1983, Absorption by Small Particles (New York: Wiley)
Edwards, D. F. & Philipp, H. R. 1985, in Handbook of Optical Constants of Solids, ed. E. D. Palik (Orlando: Academic Press), 665
Mutschke, H., Andersen, A. C., Jäger, C., Henning, T., & Braatz, A. 2004, A&A, 423, 983
Neugebauer, G., Green, R. F., Matthews, K., Schmidt, M., Soifer, B. T., & Bennett, J. 1987, ApJS, 63, 615
Scott, J., Kriss, G. A., Brotherton, M. S., Green, R. F., Hutchings, J., Shull, J. M. & Zheng, W. 2004, ApJ, 615, 135
Shang, Z., Brotherton, M. S., Green, R. F., Kriss, G. A., Scott, J., Quijano, J. K., Blaes, O., Hubeny, I., Hutchings, J., Kaiser, M. E., Koratkar, A., Oegerle, W., & Zheng, W. 2005, ApJ, 619, 41
Telfer, R. C., Zheng, W., Kriss, G. A., & Davidsen, A. F. 2002, ApJ, 565, 773 (TZ02)
Van Kerckhoven, C., Tielens, A. G. G. M., & Waelkens, C. 2002, A&A, 384, 568

Luc Binette, Yair Krongold and Jose Antonio de Diego: Instituto de Astronomía, Universidad Nacional Autónoma de México, Ciudad Universitaria, Apartado Postal 70–264, CP 04510, México D.F., México (LBinette@astroscu.unam.mx).
Gladis Magris Crestini: Centro de Investigaciones de Astronomía, Apartado postal 264, Mérida 5101-A, Venezuela